Local Dynamic Similarity Concept as Applied to Evaluation of Discharge Coefficients of Cross-Ventilated Buildings - Part 1 Basic Idea and Underlying Wind Tunnel Tests; Part 2 Applicability of Local Dynamic Similarity Concept; Part 3 Simplified Method for Estimating Dynamic Pressure Tangential to Openings of Cross-Ventilated Buildings

Takashi Kurabuchi[1], Masaaki Ohba[2], Tomonobu Goto[2], Yoshihiko Akamine[3], Tomoyuki Endo[1] and Motoyasu Kamata[3]

[1]Tokyo University of Science, Japan
[2]Tokyo Polytechnic University, Japan
[3]University of Tokyo, Japan

Abstract

A model has been proposed for evaluating the discharge coefficient according to the flow angle at an inflow opening for cross-ventilation. This model is based on the fact that the cross-ventilation flow structure in the vicinity of an inflow opening creates dynamic similarity under the condition that the ratio of cross-ventilation driving pressure to dynamic pressure of cross flow at the opening is consistent. It was confirmed from a wind tunnel experiment that the proposed model can be applied almost regardless of wind direction and opening position. Change of pressure along the stream tube of a cross-ventilated flow was estimated from the results of Large Eddy Simulation, and was set as the basis of model preparation.

In order to perform detailed evaluation on the applicability of the local dynamic similarity concept, wind tunnel experiments were conducted under conditions where the opening positions and the arrangement of buildings were changed. As a result, it was found that the discharge coefficient C_d can be predicted accurately from P_R* for most of the opening positions, even if the approaching flow angle is varied or another building is standing near the opening. It was also found that there are no substantial problems for predicting C_d from P_R* when the direction of interfering cross flow is changed or there is wall/floor near the opening disturbing the diffusion of incoming airflow. However, it should be noted that the prediction accuracy of C_d is lowered when these conditions occur simultaneously.

To predict the ventilation flow rate based on the local dynamic similarity model, it is necessary to estimate the value of dynamic pressure tangential to openings (P_t). A simplified method was investigated for estimating the value of P_t by Irwin's surface wind sensor. The wind velocity tangential to the wall measured by this sensor was broadly consistent with the value measured by a hot-wire anemometer. Moreover, P_t calculated from the wind velocity measured by the surface wind sensor was compared with the differential pressure between total pressure (P_T) and wind pressure (P_W) measured directly at the opening. They were broadly consistent with each other. From these results, it is concluded that we can estimate the value of P_t by the surface wind sensor very simply.

Key words: Local dynamic similarity model, ventilation flow rate, inflow opening, total pressure, wind tunnel experiment, CFD, LES, cross-ventilation, discharge coefficient, inflow angle, dynamic pressure.

1. Introduction

In recent years, there has been considerable interest and concern about the utilization of airflow for improving indoor thermal conditions in hot and humid rooms, which is important for energy-saving in buildings. To expand the use of natural ventilation and to establish a reliable and effective utilization method, a much more profound understanding of the mechanism of natural ventilation and, in particular, cross-ventilation is required.

In this paper the nature of the discharge coefficient which relates wind pressure and ventilation flow rate is examined by both CFD modelling and wind tunnel experiments. In particular, the variation of discharge coefficient with wind direction is investigated. The work is based on the authors' published work (Kurabuchi et al., 2004) and newly conducted wind tunnel experiments. The paper is divided into three. Part one, described in Section 2, considers basic ideas which show how the dynamic similarity model and wind tunnel tests can be used to determine how the discharge coefficient for an opening changes with wind direction and opening position for a simple building shape. Part 2 (Section 3) considers more complex situations with a wider selection of opening positions and different building layouts. The third part (Section 4) describes measurements of the wind velocity tangential to an opening and its relationship to the total pressure at the opening.

2. Part 1. Basic Ideas and Underlying Wind Tunnel Tests

Conventionally the orifice equation generally used for the estimation of flow rate, Q, for natural ventilation is given by:

$$Q = C_d A \sqrt{\frac{2}{\rho}(P_W - P_R)} \qquad (1)$$

where C_d is discharge coefficient, A is opening area, P_R is room pressure, and P_W is wind pressure.

However, wind tunnel experiments have demonstrated that the discharge coefficient relating wind pressure with ventilation flow rate varies with wind direction and opening position (Vickery and Karakatsanis, 1987, Kiyota and Sekine, 1989, Sawachi et al., 2004). Therefore it is difficult to estimate ventilation flow rate from the above equation. Unfortunately, no model has yet been presented that adequately explains how the discharge coefficient is changed. Under such circumstances, the present study attempts to accurately identify ventilation phenomena through use of both experiments and CFD. In the process, it is shown that total pressure can be considered as a parameter specific to an opening in a manner similar to wind pressure. A dynamic similarity model is proposed using the total pressure at the opening in addition to wind pressure and room pressure. This is used to explain how the discharge coefficient varies.

2.1 Large Eddy Simulation Applied to Cross-Ventilation

2.1.1 Outline of CFD and Wind Tunnel Model Experiment

Cross-ventilation air flow is characterized by rapid acceleration and rapid deceleration. Because it is considered difficult to apply an eddy viscosity model such as the k-ε model (Kurabuchi et al., 2000), a Large Eddy Simulation (LES) model was used where the Smagorinsky coefficient is regarded as constant (C_s = 0.13). As shown in Figure 1, the study was performed on a ventilation airflow in a building where the boundary layer flow is regarded as an approach flow. The building under study was in the form of a rectangular parallelepiped of 2:2:1. The direction of the approach flow was varied in the range of 0 = to 67.5 degrees.

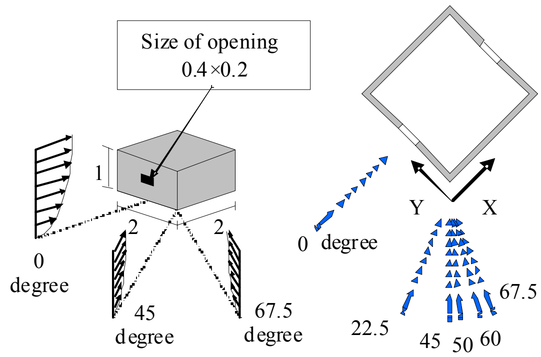

Figure 1. Building model and wind direction.

2.1.2 Determination of Stream Tube Shape

The structure of ventilation airflow was elucidated from the analysis of calculation results. First, passive markers were set out from the opening's section. By tracing these trajectories upstream and downstream, stream tube shapes before and after passing the opening were determined. When the wind direction is other than 0 degrees, the stream tube contacts the wall surface before it reaches the opening, as shown by the result of the case in Figure 2, where the wind direction is set to 45 degrees. It is turned to a flow along the wall surface and reaches the opening. This means that in most cases the ventilation air flow may be approximated by a wall jet or boundary layer flow before it flows into the opening.

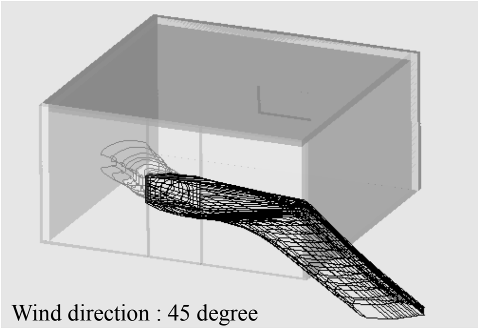

Figure 2. Shape of stream tube in the vicinity of opening.

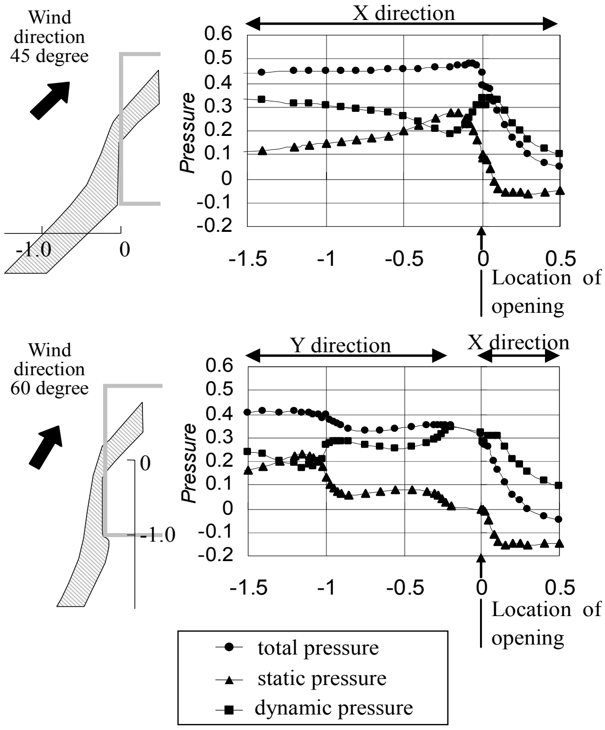

Figure 3. Identified shape of stream tube and streamwise change of pressure.

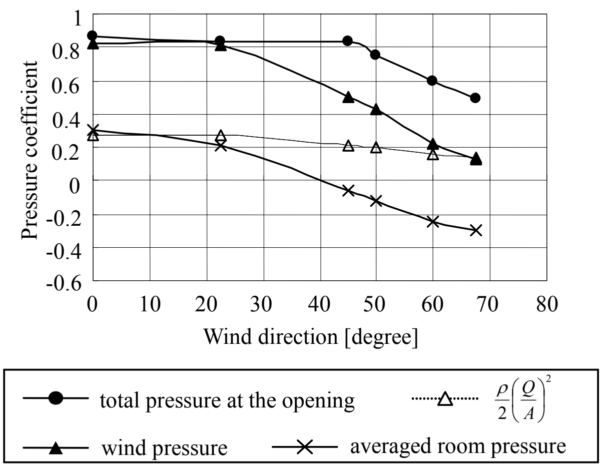

Figure 4. Evaluated pressure at different wind direction angles.

2.1.3 Pressure Change Along Stream Tube

The flow rate and weighted average values of total pressure, static pressure and dynamic pressure in each cross-section of the stream tube were calculated. The changes in these values together with the shape of the stream tube are shown in Figure 3. From this figure, it is apparent that static pressure and dynamic pressure show extreme changes before reaching the opening when the wind direction is 45 degrees or less, while the total pressure, i.e. the sum of the two, is almost constant, and pressure loss is low in the process where the wind flows along the windward wall surface. However, in the shape of the stream tube when the wind direction is 60 degrees, the flow is separated at the windward corner and the flow reattaches again to the wall, and total pressure is decreased in this process.

Figure 4 shows the changes of total pressure, wind pressure and room pressure at the opening where the approaching flow angle is changed. Until the wind direction reaches 45 degrees, the total pressure at the opening is constant. When the wind direction exceeds 45 degrees, the airflow is separated at the windward corner, and the total pressure is greatly decreased.

2.2 Local Dynamic Similarity

2.2.1 Modelling of the Flow around the Opening

Based on the results of LES, a useful model is presented, which characterizes the flow around an opening. First, for a building with cross-ventilation, total pressure at a ventilation opening is split into three components, i.e. dynamic pressure normal to the opening P_n, tangential dynamic pressure P_t, and static pressure P_S (Figure 5). Next, room pressure P_R is selected as an essential parameter on the room side. Because there is no meaning in absolute pressure, static pressure loss "P_S–P_R", which is the difference between the static pressure and the room pressure, is considered. Further, for convenience, special notice is given to "P_n+P_S–P_R", i.e. the static pressure loss plus P_n. Under the condition where the cross-ventilation flow rate becomes 0, the room pressure is equal to wind pressure P_W. In this case, $P_n+P_S=P_W$. If it is supposed that the same condition exists even when there is airflow, the value of $P_n+P_S-P_R$ can be approximated as the ventilation driving force P_W-P_R. Therefore, P_n, P_t and P_W-P_R are identified as important parameters to characterize flow around the opening.

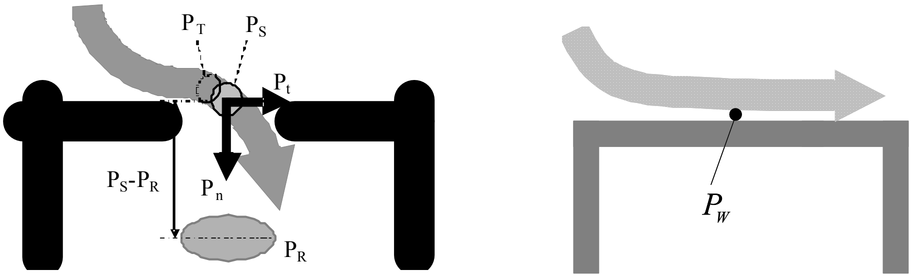

Figure 5. Characteristic pressures at opening.

Suppose the building remains the same and only the velocity of the approaching flow is doubled. Then, all of these pressure values should be quadrupled. This is because dynamic similarity of the total flow field is established. Under the condition where dynamic similarity of total flow field is established, the dimensionless values calculated by combining the three pressure values extracted above become constant. The following combinations of these dimensionless values can be considered:

- P_n/P_t corresponding to inflow angle β;
- pressure loss coefficient $\zeta_n = P_n/(P_W - P_S)$ of ventilation air related to discharge coefficient C_d.

From experiments performed by changing the approaching flow angle, the corresponding relation between the inflow angle and the discharge coefficient is determined.

In the case where air flow conditions acting around the opening can be represented by the three pressure values extracted above alone, it is expected that similarity of the flow can be established without depending on the shape of the building, position of the opening and approaching flow angle, etc. This concept is known as local dynamic similarity in the sense that dynamic similarity exists not in the total flow field but only in the vicinity of the opening. In this case, a pair of dimensionless values prepared from the three pressure values represents a specific airflow condition. If these values correspond to each other in a one to one relationship, it may be deduced that, when one of them is determined, the other is automatically determined.

In order that local dynamic similarity of the flow is established, the following conditions may be required:

a) The shape of the opening has geometrical similarity;

b) The direction of tangential flow of the approaching flow with respect to the opening is constant;

c) The opening is positioned on a wall surface which is sufficiently large with respect to the size of the opening;

d) There is no wall to hinder the diffusion of incoming air flow near the opening on the room side.

The experimental results are used to confirm how far these conditions must be satisfied in order that local similarity is established.

The inflow angle β cannot be determined unless ventilation flow rate is determined. Thus, a dimensionless room pressure P_R* is defined according to Equation (2), and this is used instead of β, i.e:

$$P_R* = \frac{P_R - P_W}{P_t} \tag{2}$$

where:
P_T is the total pressure at the opening (see Figure 5).

It is defined in such manner that it corresponds to the inflow when P_R* is negative, and it corresponds to the outflow when it is positive.

2.2.2 Validity of Suction Experiment

A quick experimental evaluation was conducted by assuming various experimental conditions for the approaching flow angle, the position of the opening, and the ventilation flow rate. A building model was connected with a suction fan on the leeward side which was exposed to the approaching flow as shown in Figure 6. To evaluate whether the actual ventilation condition can be correctly reproduced by this experimental setup, the suction airflow rate was adjusted to achieve the same room pressure for each shown in Figure 1, where both room pressure and

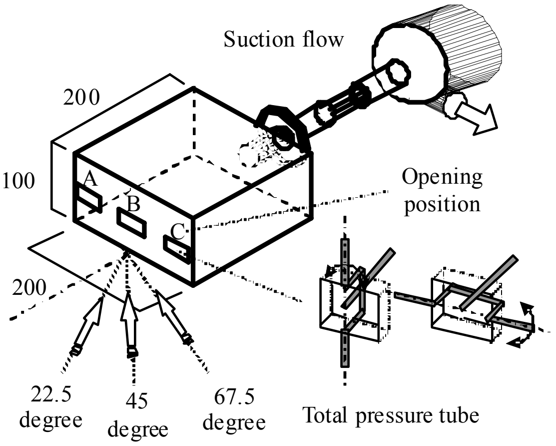

Figure 6. Experimental setup to evaluate validity of local dynamic similarity concept (unit:mm).

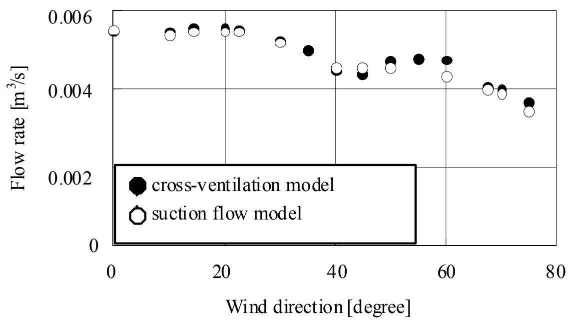

Figure 7. Comparison of suction flow rate and actual cross-ventilation flow rate.

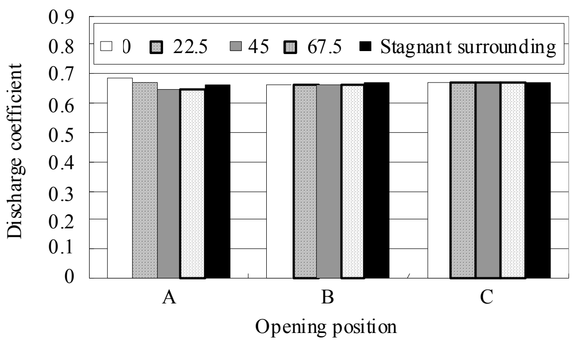

Figure 8. Comparison of Cd's in case of P_R^*→-∞.

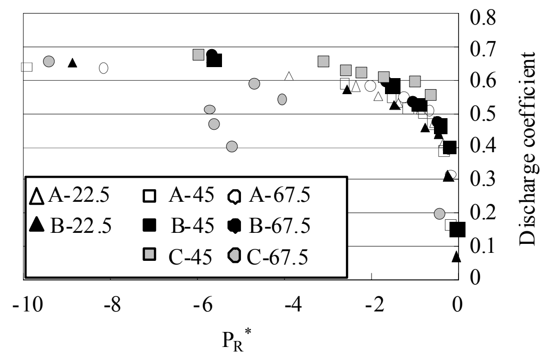

Figure 9. Discharge coefficient curves as a function of P_R^* for different wind direction angles and opening locations.

approaching flow angle of the ventilation model cross-ventilation flow rate had already been measured. The results are as shown in Figure 7. Because flow rate showed good matching, it is possible to determine ventilation performance at the opening during ventilation by this method.

2.2.3 Validity of Local Dynamic Similarity Concept

To evaluate the validity of the proposed model, a wind tunnel experiment was conducted as shown in Figure 6 by setting the position of the opening and the wind direction as variable, and the corresponding relation between P_R^* and discharge coefficient was assessed. It was assumed that the openings were located at 3 positions at the central height. The end of the opening closest to the side wall concurred with the side wall, and this may have conflicts with the precondition (d) as given above (see Section 2.2.1).

First, it was evaluated whether the discharge coefficients (C_d) always concurred in the case $P_R^* \to -\infty$. Two extreme cases were assumed: a case where stagnant surrounding conditions exist around the opening and P_t=0 and suction is performed by using a fan, and a case where the approaching flow angle is considered and the suction flow rate is assumed to be large enough to achieve $P_n >> P_t$. The results of the comparison for each opening are summarized in Figure 8. From this Figure, it was confirmed that discharge coefficients concur well for all of the openings.

Next, measurements were performed under the condition where the value of P_t cannot be neglected. It was difficult to obtain the value of P_t at the ventilation opening from the measurement of wind velocity. In this respect, the following method was adopted which did not depend on direct measurement. Total pressure P_T at the opening is $P_n+P_t+P_s$. If it is assumed that the value of P_w approximates the value of $P_n + P_s$, the value of P_t can be evaluated as:

$$P_t = P_T - P_W$$

and Equation (2) becomes:

$$P_R^* = \frac{P_R - P_W}{P_t} = \frac{P_R - P_W}{P_T - P_W} \qquad (3)$$

By assuming that the value of P_w can be substituted by the room pressure when the ventilation flow rate is 0, the value of P_T was determined by directly measuring the value at the centre of the opening using the total pressure tube.

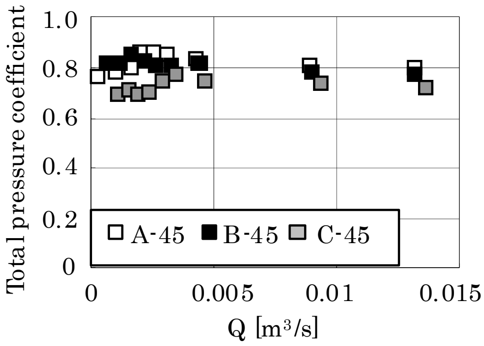

Figure 10. Relationship betweeen total pressure coefficient and suction flow rate.

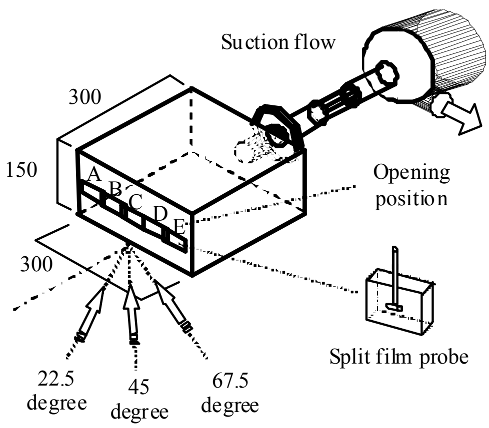

Figure 11. Experimental setup to evaluate the relation between discharge coefficient and inflow angles with P_R^* (unit:mm).

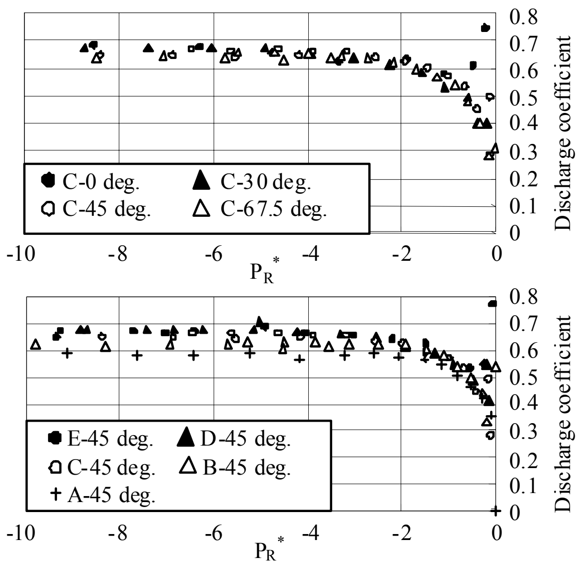

Figure 12. Discharge coefficient curves for different wind direction angles and opening locations.

The relation between P_R* and C_d is shown in Figure 9. In the figure, the value of P_T as measured for each ventilation flow rate was used. The results, shown in Figure 9, confirm that the relation between these two values can be represented by the same curve except for some cases. There was extensive deviation from the curve in the case where the approaching flow angle was 67.5 degrees at the windward end. In this case, there are two possibilities: the flow was separated near the opening and total pressure could not be measured accurately, and there were conflicts with precondition (b) given in Section 2.2.1. Also, in the case where the approaching flow angle was 22.5 degrees at the windward end, the values of total pressure P_T and the wind pressure P_W were very close to each other. It was difficult to evaluate the value of P_t in this experiment, and this was exempted from the study. Except for these cases, it was confirmed that local dynamic similarity could be established under extensive conditions regardless of the position of the opening and the approaching flow angle.

2.2.4 Simplification to Assume Total Pressure

If it is necessary to have the value of P_T corresponding to the ventilation flow rate prior to the prediction of discharge coefficient, a practical predicting method cannot be established. However, the value of P_T measured in the above experiment takes a nearly constant value without depending on the ventilation flow rate as shown in Figure 10. In this respect, an attempt was made to simplify the measurement by using the value of P_T without depending on the ventilation flow rate when suction flow rate was increased as much as possible so that an inflow angle of about 90 degrees could be postulated. To evaluate the validity of this method, a wind tunnel experiment was conducted by using a building model similar to the model used in the previous experiment as shown in Figure 11. Here, for the purpose of assessing unique matching between P_R^* and the inflow angle β, the inflow angle at the centre of the opening was measured by using a split film probe.

2.2.5 Verification of Model Validity

In order to verify the validity of the proposed model, the relation between C_d and P_R* is shown in the upper figure in Figure 12, which summarizes a case where the wind direction was changed and the position of the opening was fixed at the front centre of the building (opening position C). In the lower

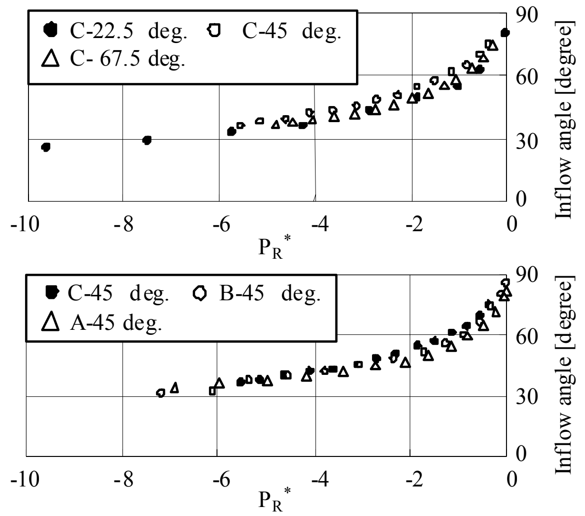

Figure 13. Inflow angle curves for different wind direction angles and opening locations.

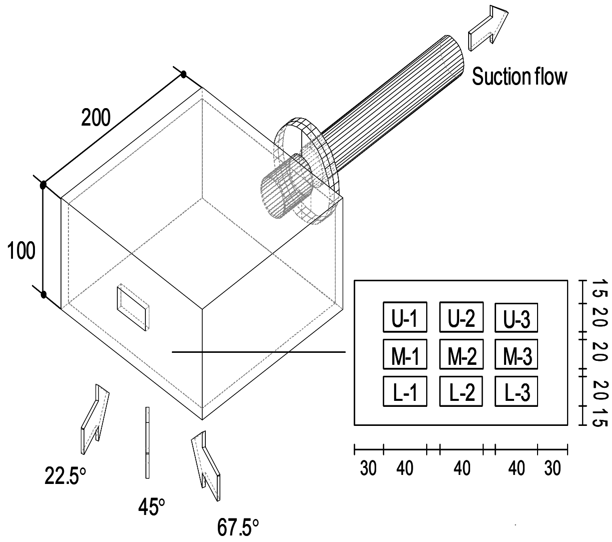

Figure 14. Suction type ventilation model and opening positions (scale: mm).

figure in Figure 12, the relation where the wind direction was fixed at 45 degrees and the position of the opening was changed is shown. According to this figure, when P_R* is less than -5, C_d is almost constant. When it is -2 or more, C_d tends to decrease rapidly. This relation remains almost constant regardless of the position of the opening and the wind direction. Similarly, Figure 13 shows the relation with the inflow angle at the centre of the opening when wind direction and the position of the opening are changed. When P_R* increases, β approaches 90 degrees. In this way, by applying this local dynamic similarity model, it is experimentally demonstrated that the changes of C_d and β can be explained by a single parameter P_R^*.

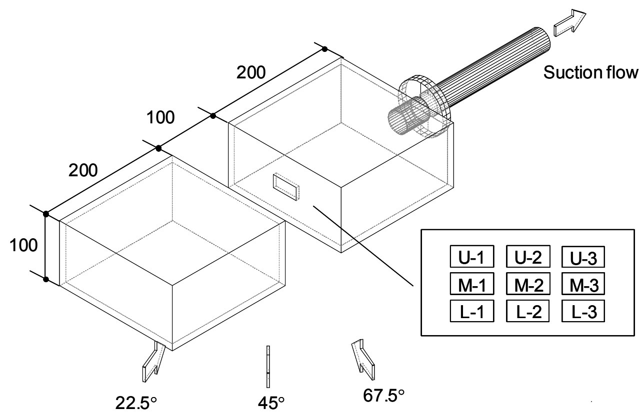

Figure 15. Layout of two building models.

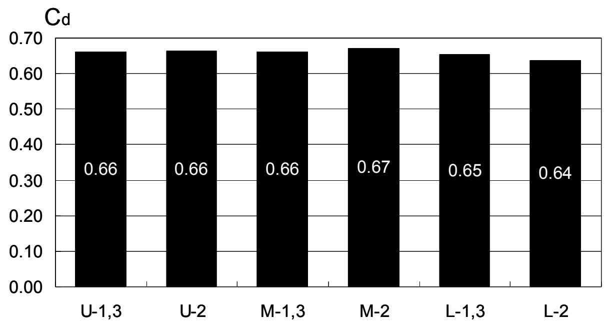

Figure 16. Discharge coefficients (C_d) in case of $|P_R^*|=\infty$.

3. Part 2. Applicability of Local Dynamic Similarity Concept

In this section, from the viewpoint of the application to actual buildings, wind tunnel experiments were carried out under some extended conditions where the opening position and building position were changed, and the application range of the local similarity concept was investigated.

3.1. Wind Tunnel Experiment for Various Opening Positions and Different Building Layouts

The experiment was carried out by using the Eiffel type of wind tunnel at Tokyo Polytechnic University and the building model as shown in Figure 14.

In the present experiment, the opening position was widely changed when compared to Part 1. As shown in Figure 14, nine opening positions were designed, and three opening positions were located at different heights on the wall. To test more complicated conditions, another building model was placed on the windward side of the building model as shown in Figure 15, and an experiment on the same opening positions was also performed. The opening position was changed by replacing the panel on the windward side of the building model.

As already described in Part 1, for the purpose of simulating various ventilation flow rates, a duct was connected on the leeward side of the model, and the ventilation flow rate was controlled by a suction fan installed outside the wind tunnel. The ventilation flow rate was measured by a thermal flow meter mounted on the middle of the duct. P_T was measured with a total pressure tube positioned at the centre of the opening, and P_R was measured at the ceiling surface of the building model. The approach flow was a boundary layer flow with a power-law index of 0.25, and the reference velocity was kept at 7.0 m/s at the upwind edge of the model. The incident angle of approach flow was set to 22.5°, 45°, and 67.5°.

First of all, C_d was measured under the stagnant condition without approach flow, where $|P_R^*|$ was considered to be infinity. It was found that the value was distributed between 0.64 and 0.67 and was almost constant as shown in Figure 16.

Then, the relationship between P_R^* and C_d was observed at each opening position and each incident angle of approach flow with changing ventilation flow rate. This relationship is shown in Figures 17, 18 and 19 for each height of the opening positions. In these figures, a basic line is also depicted, which indicates the relationship between P_R^* and C_d at the basic opening position M-2. Figure 18 shows that the relationship between P_R^* and C_d at the openings

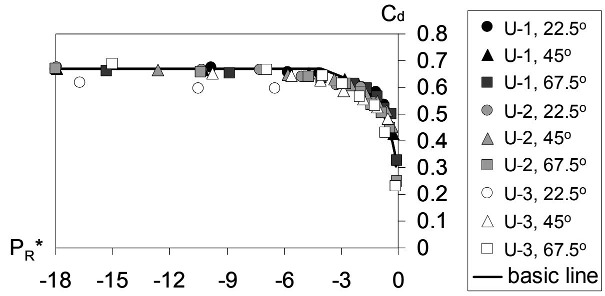

Figure 17. Relationship between P_R and C_d at upper openings.*

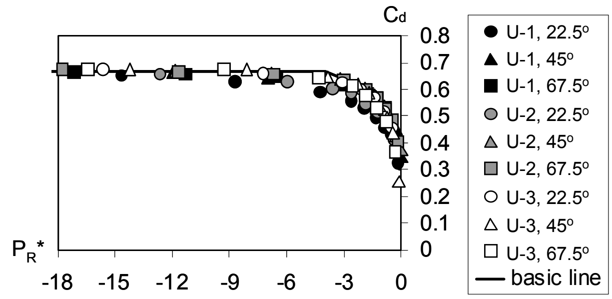

Figure 20. Relationship between P_R and C_d at upper openings faced toward another building.*

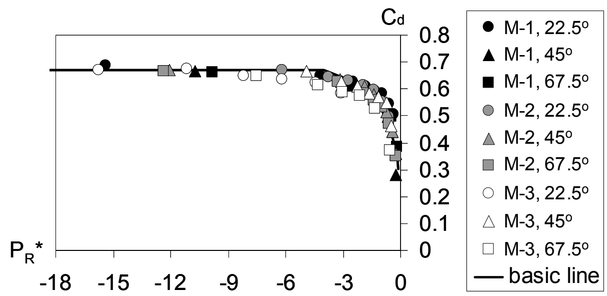

Figure 18. Relationship between P_R and C_d at middle openings*

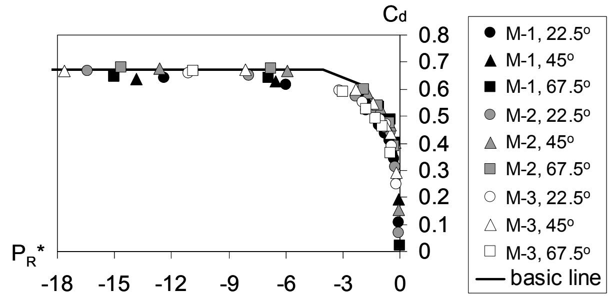

Figure 21. Relationship between P_R and C_d at middle openings faced toward another building*

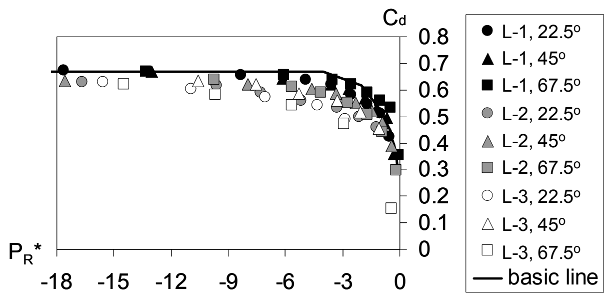

Figure 19. Relationship between P_R and C_d at lower openings.*

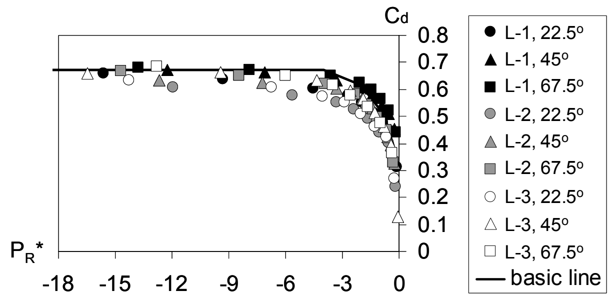

Figure 22. Relationship between P_R and C_d at lower openings faced toward another building.*

of the middle height is the same as in the basic line. At the upper openings, the value of C_d was also consistent with the basic line, although C_d of U-3 was a little lower when the incident angle was 22.5°. However, the C_d corresponding to $|P_R^*|$ tended to be smaller at the lower openings than that of the basic line. This trend was more obvious in the opening position on the windward side.

Next, the results of the experiment when another building model was placed on the windward side of the building model are shown in Figures 20, 21 and 22. As shown in these figures, the relationship between P_R^* and C_d at the upper and middle openings was almost consistent with the basic line, while the C_d corresponding to $|P_R^*|$ tended to be smaller at the lower openings than that of the basic line. These were the same findings as in the case of the isolated building model.

3.2 Influence of Crossflow Direction and Internal Wall on the Application of Local Dynamic Similarity Concept

The results of the experiment as described above confirms that it is possible to evaluate C_d by using P_R^* as an index for most of the opening positions, even if another building is standing in front of the opening. However, when the opening was located in the lower part of the wall, the C_d corresponding to $|P_R^*|$ tended to be smaller than that of the basic line.

This might be attributed to the fact that the direction of the interfering crossflow on the lower area of the wall was not parallel to the floor. Instead it was diagonal to downward, while the direction of the interfering crossflow on the upper area was primarily parallel to the floor. This conflicts with one of the requirements needed to establish the local dynamic similarity concept, which were described in Section 2.2.1.

In order to confirm this, an additional experiment was undertaken, and the opening at the basic position of M-2 was rotated as shown in Figure 23. As a result, it was found that the direction of the interfering crossflow influences the relationship between P_R^* and C_d as shown in Figure 24.

However, as shown in Figure 19 or Figure 22, C_d was rather lower than the case where the opening was rotated at an angle of 90°. Therefore, there might be another effect caused by the floor near the opening on the room side, which disturbed the diffusion of the incoming airflow. This is also a factor in conflict with the requirements of the local dynamic similarity concept.

In order to confirm this effect, a partition wall or double floor was installed in the building model. The partition wall was located on the leeward side or windward side of the basic opening M-2, and the double floor was provided on the lower end of the opening as shown in Figure 25.

Figure 26 shows C_d with the inclusion of the inside wall or floor when the value of $|P_R^*|$ is infinity. It was found to be lower than that without the inside

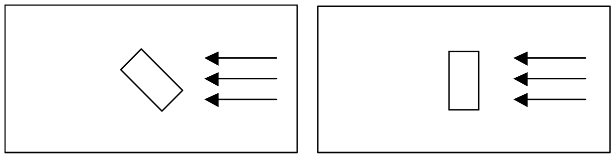

Figure 23. Rotated openings (left: 45°, right: 90°).

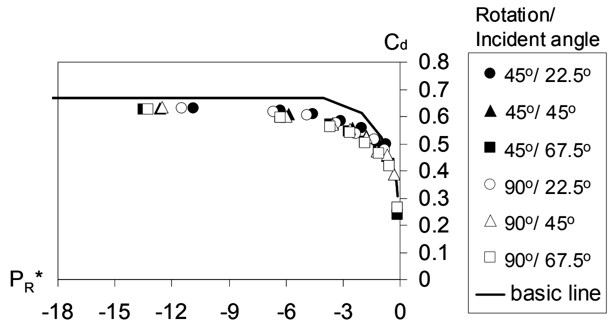

Figure 24. Relationship between P_R^* and C_d at rotated openings.

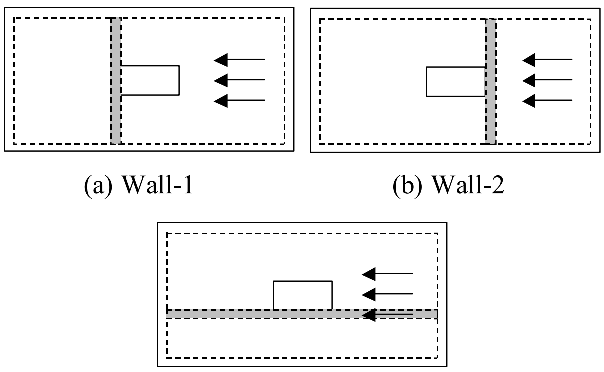

(a) Wall-1 (b) Wall-2

(c) Double floor

Figure 25. Partition wall and double floor inside the building model.

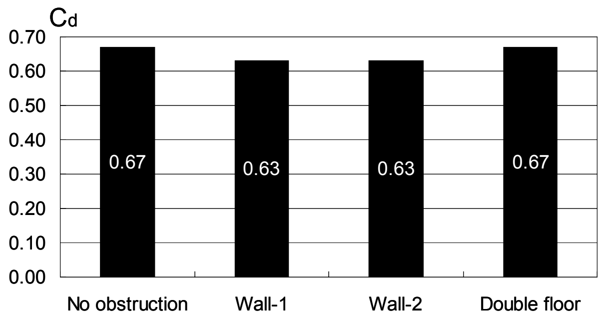

Figure 26. Discharge coefficients (C_d) of openings with partition wall or double floor in the case of $|P_R*|=\infty$.

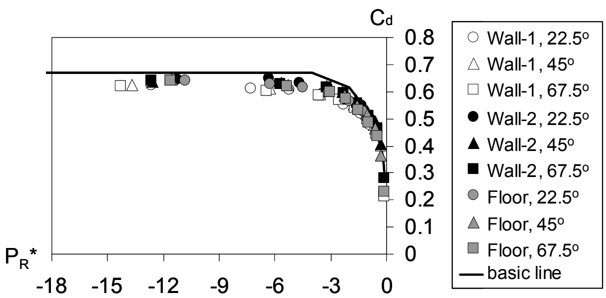

Figure 27. Relationship between P_R* and C_d at openings with partition wall or double floor.

wall or floor, but the difference was only 0.04. As shown in Figure 27, C_d tends to be lower than the basic line under all conditions and that is most obvious when the wall was installed on the leeward side, i.e. when the wall was standing against the incoming airflow.

As shown in Figures 24 and 27, the difference of C_d from the basic line was only up to 0.1 under those conditions. Thus, it would not be a substantial problem when we apply the present concept, in practice, to those conditions. However, it should be known that the prediction accuracy of C_d is lowered when these conditions simultaneously occur such as in the case of the openings on the lower part of the wall in this study.

4. Part 3 Simplified Method for Estimating Dynamic Pressure Tangential to Openings

To determine the parameter P_R*, given in Equation (3), it is necessary to determine P_t or P_T in addition to P_W. When the position of the opening is determined, it is possible to estimate the value of P_T by pitot-tubes directly, as already reported in Part 1 (Section 2). However, when we consider "the determination of the opening -position during the design stage", this measuring method is not suitable for practical application. So, this section addresses the issue of a simplified method for estimating P_t by using the surface wind sensor developed by Irwin (Irwin, 1981).

4.1 Irwin's Surface Wind Sensor

Irwin's surface wind sensor has been developed for measuring wind velocity within a horizontal plane at the level of pedestrians in a wind tunnel model (Irwin, 1981). It is possible to estimate wind velocity at an arbitrary height from the pressure difference in the vertical direction near the floor surface independently of the wind angle. Figure 28 shows the outline of the surface wind sensor used in the present study.

A pressure-sensor-hole is provided to enclose a pressure-sensor-tube. The heights of sensor-tubes used in this study were 3 mm and 5 mm. By using the pressure-difference between the sensor–tube and sensor–hole, the wind velocity is obtained from

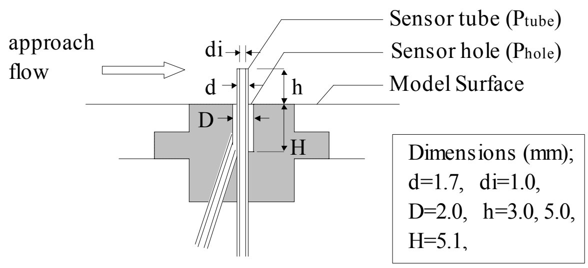

Figure 28. Geometry of the surface wind sensor.

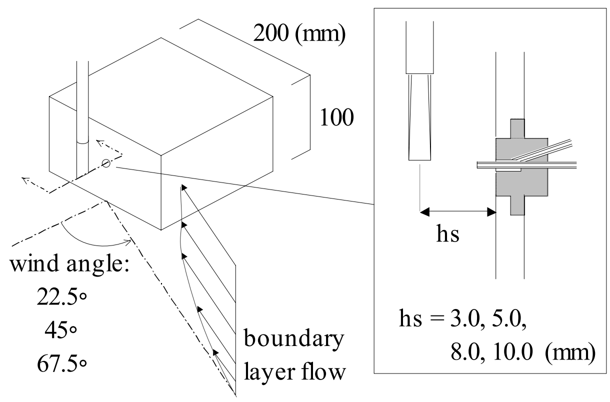

Figure 29. Outline of the experiment for calibration of the surface wind sensor.

Equation (4). Regression coefficient α and β are constants determined by airflow characteristics.

$$U_t = \alpha + \beta \times \sqrt{P_{hole} - P_{tube}} \qquad (4)$$

where:

U_t: Wind velocity tangential to the wall
P_{hole}: Pressure measured by sensor-hole
P_{tube}: Pressure measured by sensor-tube
α, β: Regression coefficients

In this paper, these sensors were installed at the centre of the wall surface, and the values were calibrated for wind angles of 22.5º, 45º and 67.5º, as shown in Figure 29. The hot-wire anemometer was installed from above the model so that the probe was at a position perpendicular to the wall surface. The approach-flow was a boundary layer flow, and the wind velocity was varied by the wind-tunnel-fan. Regression coefficients for the height (hs) and the wind angle are shown in Table 1.

4.2 Outline of Experiment for U_t and P_t Measurements

The outline of the experiment for U_t and P_t measurement is shown in Figure 30. The approach flow was a boundary layer flow with a wind velocity of 7 m/s at the top edge of the model. Here, it is assumed that wind velocity and wind velocity pressure at the top edge of the model are standard wind velocity and standard pressure, respectively. Subsequently, standardized values based on these

Table 1. Regression coefficients of surface wind sensors.

h	hs	Wind angle (deg.)	α	β
3	3	22.5	0.09	1.31
		45	0.17	1.36
		67.5	0.13	1.49
	5	22.5	0.12	1.25
		45	0.19	1.4
		67.5	0.18	1.51
	8	22.5	0.07	1.21
		45	0.23	1.39
		67.5	0.17	1.55
	10	22.5	0.1	1.18
		45	0.22	1.39
		67.5	0.22	1.56

h	hs	Wind angle (deg.)	α	β
5	3	22.5	0.09	1.24
		45	0.11	1.31
		67.5	0.07	1.43
	5	22.5	0.12	1.19
		45	0.13	1.34
		67.5	0.11	1.45
	8	22.5	0.07	1.15
		45	0.17	1.32
		67.5	0.1	1.49
	10	22.5	0.1	1.12
		45	0.16	1.33
		67.5	0.15	1.5

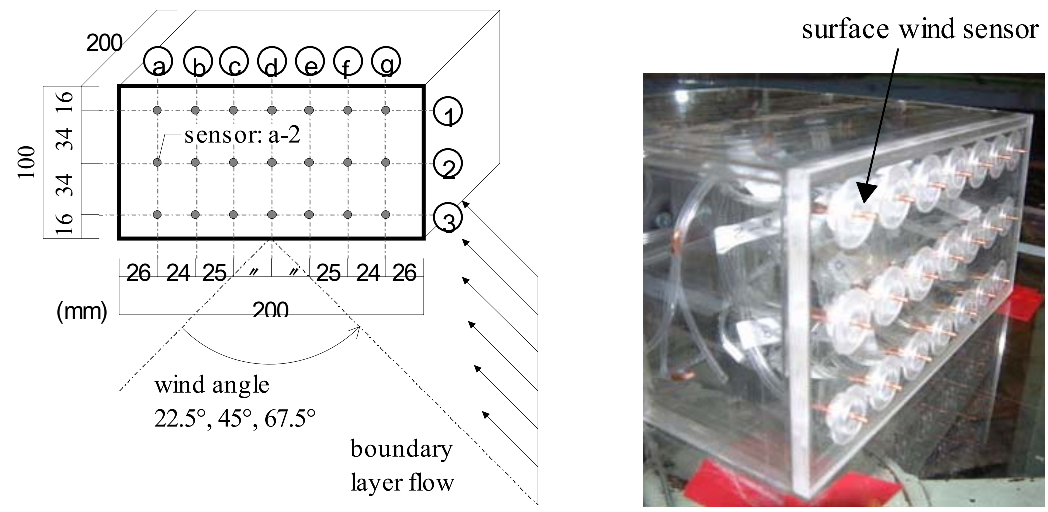

Figure 30. Outline of experiment for U_t measurement by using the surface wind sensor.

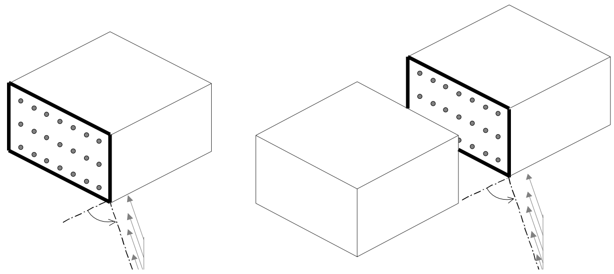

Figure 31. Model arrangements.

values are used in all parameters for wind velocity and pressure. The wind angles examined in this study were 22.5º, 45º and 67.5º. The wall surface to be evaluated was on the upstream side, and was installed with 21 measuring points. The measurement of U_t was performed by the hot-wire anemometer and the surface wind sensor. The measuring method of the hot-wire anemometer was identical to that of the sensor calibration. The sensor pressure was measured simultaneously at all points by a multi-point pressure-transducer. Measurements were made on the model with two arrangements as shown in Figure 31, i.e. the model alone (Case 1) and the model with another one in front of the wall surface to be evaluated (Case 2).

4.3 Result and Discussion

4.3.1 Interference between Sensors

Prior to the measurement of U_t and P_t, the influence of interference between sensors when measurements were made simultaneously at 21 points was confirmed. For measurement point a-2 (see Figure 30), the differential pressure between P_{hole} and P_{tube} measured individually and simultaneously along with other sensors are compared in Figure 32. There was almost no difference between the two cases. Therefore, the results of subsequent measurements were determined simultaneously for all 21 points.

4.3.2 Wind Velocity Tangential to Wall (U_t)

In Figure 33, the values of U_t measured by the surface wind sensor (at height h=3mm and 5mm) are compared with the values measured by the hot-wire anemometer. The measuring position was 5 mm from the wall surface. For each wind angle, in Case 1, the results were broadly consistent with the hot-wire anemometer results. In Case 2, however, the results were not as consistent as in Case 1. This may be attributed to the fact that the airflow characteristics near the measuring point are very complicated on the windward model and error may have occurred due to the directivity of the hot-wire anemometer. When the measurement results of the sensor were compared with those of the hot-wire anemometer at other positions from the wall surface, similar results were obtained.

4.3.3 Wind Pressure

The sensor-hole was located at the same position as in the wind pressure measurement. If it is supposed that wind pressure can be simultaneously measured by the sensor-hole, the efficiency of the parameter-measurement for the prediction of ventilation flow rate can be extensively improved. Wind pressure directly measured is compared with P_{hole} as shown in Figure 34. These figures indicate that P_{hole} is broadly consistent with the wind pressure. Therefore, it is possible to apply P_{hole} to wind pressure.

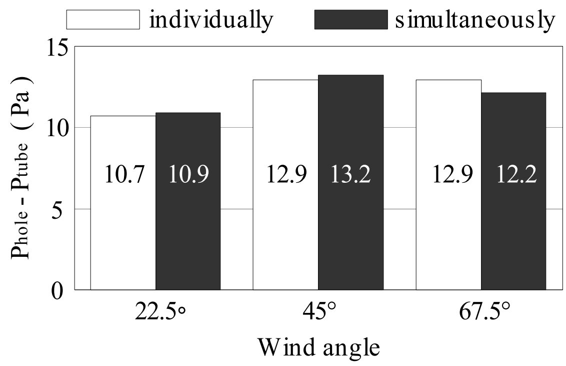

Figure 32. Comparison of P_{hole}-P_{tube} measured individually or simultaneously at point a-2.

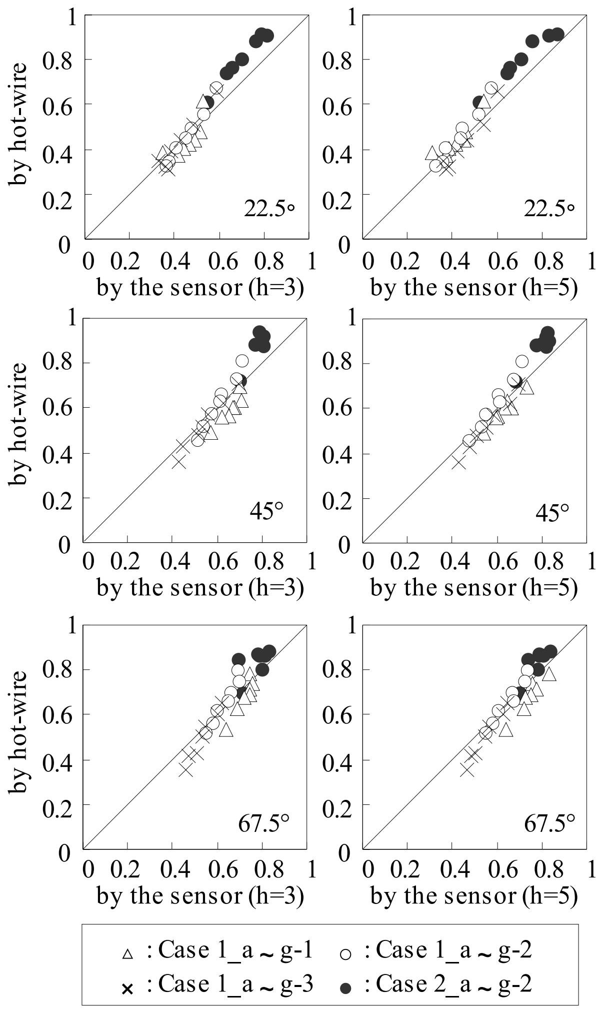

Figure 33. Comparison of U_t measured by surface wind sensor and hot-wire anemometer 5mm away from the wall surface.

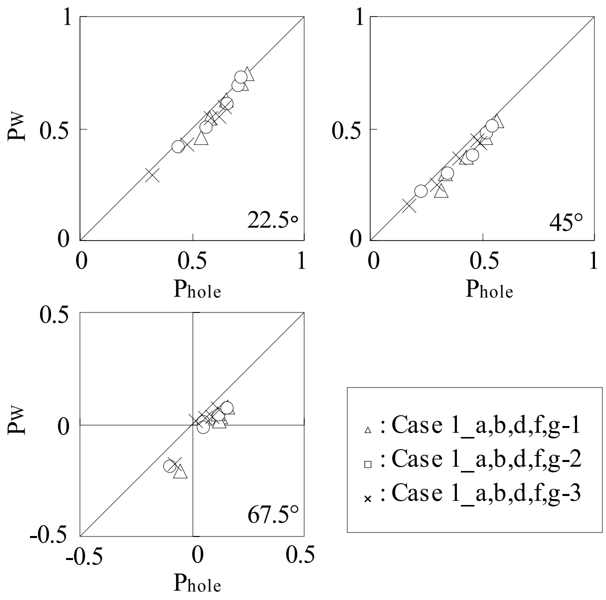

Figure 34. Comparison of P_{hole} and P_W.

4.3.4 U_t Distribution Near the Wall Surface

In predicting ventilation flow rate, the question arises of how far from the wall surface should the wind velocity be determined. If it is supposed that the value of P_T, directly measured by the pitot-tube at the opening, is the correct value, P_t can be obtained by subtracting P_W from P_T, and U_t can be determined. The U_t distribution near the wall surface at the central height of the model in Case 1 is shown in Figure 35. This figure shows the results of U_t calculated backward from P_T directly measured at the opening, measured by the sensor and the hot-wire anemometer. U_t measured by the sensor and the hot-wire anemometer were very high values on the windward side compared to the value calculated backward from P_T. When the wind angle is 22.5° and the measuring point is near the collision area of the approach flow (e.g. g-2), it is difficult to perform measurements because of the structure of the surface wind sensor. When the wind angle is 67.5° there may be an influence from separation flow at the windward end of the model (e.g. g-2).

A point from the wall surface where U_t is consistent with the value calculated backward from P_T changes according to the wind angle and the position of the wall surface. Therefore, it is difficult to decide the point to measure U_t. More study on this subject is necessary, considering the error in the prediction of ventilation flow rate.

4.3.5 Wall Surface Distributions of P_t, P_W, and P_T

Wall surface distributions of P_t, P_W, and P_T measured directly at the opening and measured by the surface wind sensor (h=5 mm) in Case 1 and Case 2 are shown in Figure 36 and Figure 37 respectively.

The distribution of P_t is obtained from the difference between P_T and P_W directly measured at the opening and from wind velocity 5 mm away from the wall surface measured by the sensor. The distribution of P_T is obtained from direct-measurement at the opening and the sum of P_t and P_W measured by the sensor. The sensor results were broadly consistent with those measured directly at the opening for each pressure parameter and case. Thus, it was confirmed that a simplified estimation of P_t and P_T could be measured by using the surface wind sensor.

However, for measurement accuracy, it is necessary to consider the error in the prediction of the ventilation flow rate.

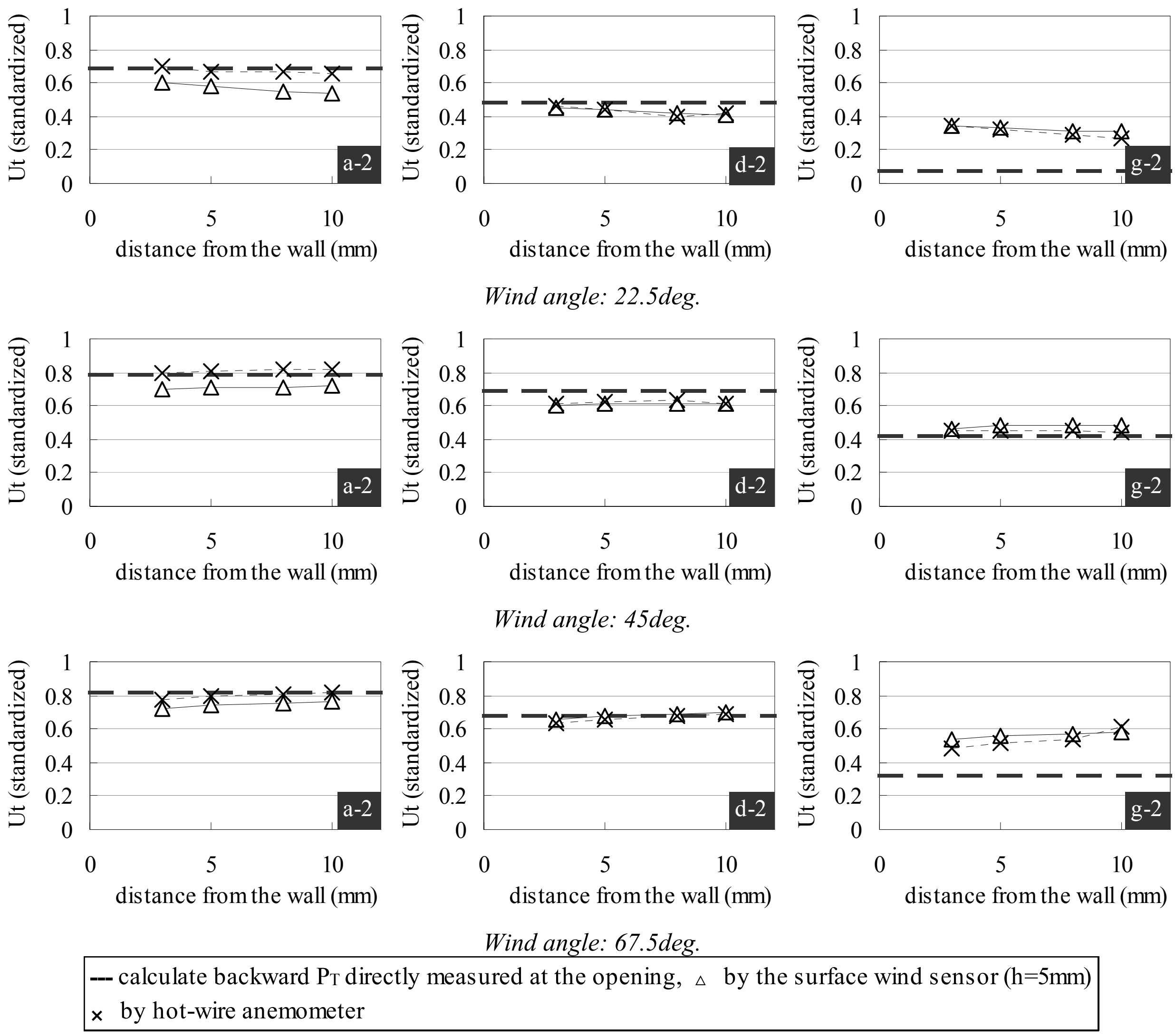

Figure 35. U_t distribution near the wall surface at points a-2, d-2, and g-2.

The time required for direct measurement of P_T distribution on the wall surface of all wind angles was about 30 hours. In contrast, when the sensor was used, the time required was only 1.5 hours including the time for calibration of the sensor.

5. Conclusions

The findings of Part 1 of this study can be summarized as follows:

- Before the ventilation airflow reaches the opening, the total pressure of the approach flow is preserved almost completely regardless of the approaching flow angle if flow separation does not occur before it reaches the opening.
- The dynamic structure of the ventilation airflow becomes similar where dimensionless indoor pressure P_R* is consistent, which is expressed by the ratio of the ventilation driving force to the difference between total pressure and wind pressure at the opening.
- When P_R* is constant, the inflow discharge coefficient is consistent with the inflow angle even when the approach flow angle and the position of the opening are changed.

From Part 2 of the study it can be concluded that:

- The discharge coefficient C_d could be predicted accurately from P_R* for most opening positions. This was the case, even if the approaching flow angle is varied or another building is standing near the opening.
- Under the condition where the direction of interfering crossflow was varied or there is any

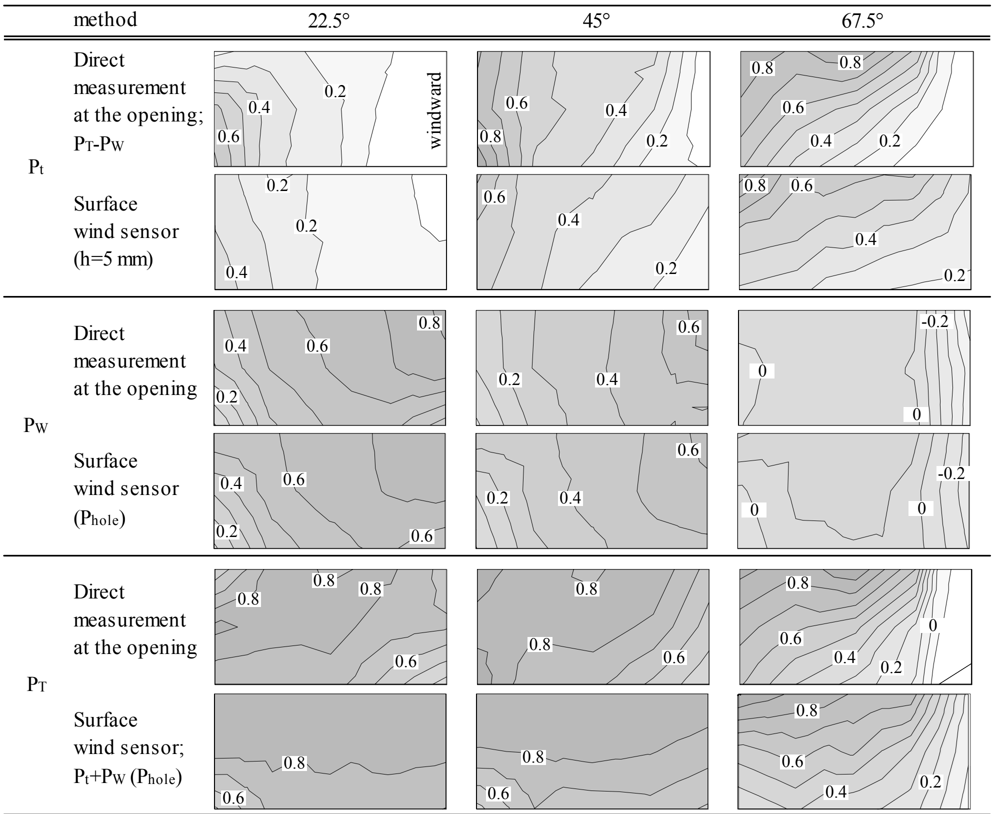

Figure 36. Wall surface distributions of P_t, P_W, and P_T measured directly at opening and measured by surface wind sensor (h=5 mm) in Case 1.

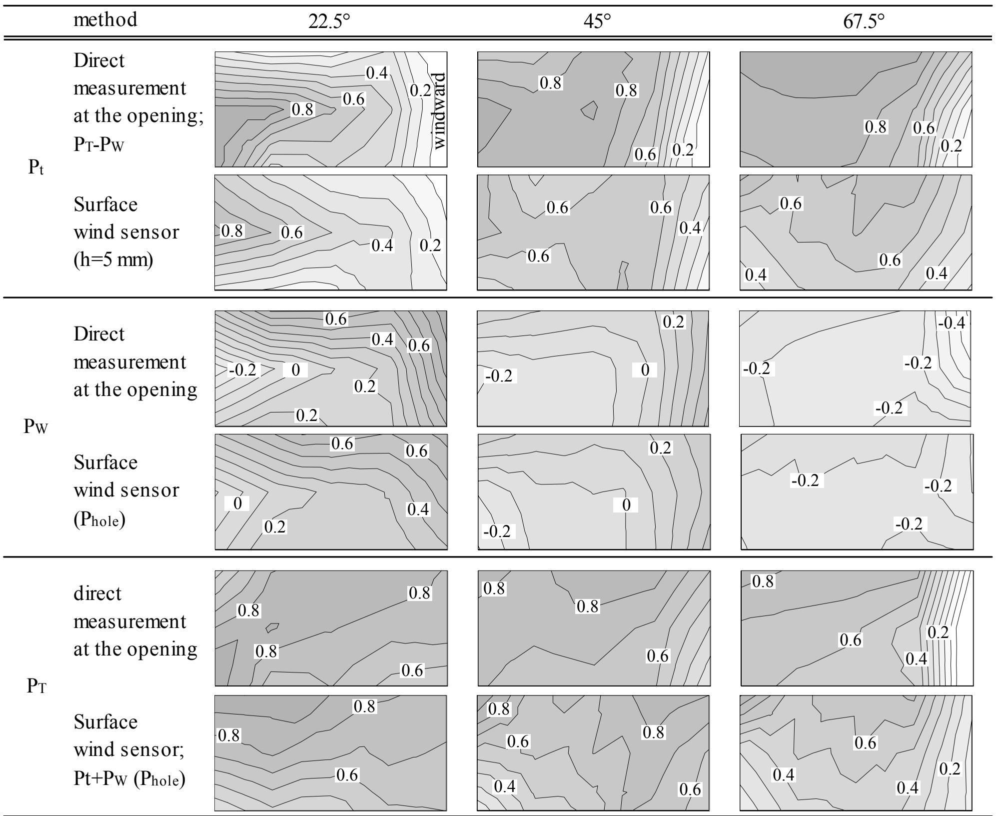

Figure 37. Wall surface distributions of P_t, P_W, and P_T measured directly at opening and measured by surface wind sensor (h=5 mm) in Case 2.

inside wall/floor disturbing diffusion of incoming flow, the C_d corresponding to $|P_R*|$ tends to be slightly smaller than that in the basic relation.

- Those conditions respectively cause no substantial problem for predicting C_d from P_R*. However, it should be noted that the prediction accuracy of C_d is lowered when those conditions occur simultaneously.

From the findings of Part 3, an investigation of a simplified method for estimating P_t with Irwin's surface wind sensor, it was concluded that:

- Wind velocity tangential to the wall surface can be measured by using a surface wind sensor.
- Pressure measured by a sensor-hole can be evaluated as wind pressure.
- P_t and P_T measured by the sensor are broadly consistent with the results measured directly at the opening.

As described above, by using a surface wind sensor, pressure parameters required for the prediction of ventilation flow rate based on the local dynamic similarity model can be simply measured.

Acknowledgement

This study was partially funded by the Ministry of Education, Culture, Sports, Science and Technology, Japan, through the 21st Century Center of Excellence Program of Tokyo Polytechnic University.

Notation

A	opening area
C_d	discharge coefficient
Q	ventilation flow rate
P_n	dynamic pressure normal to wall
P_R	room pressure
P_R*	dimensionless room pressure
P_t	dynamic pressure tangential to wall
P_T	total pressure
P_W	wind pressure
U_t	wind velocity tangential to the wall
P_{hole}	pressure measured by sensor-hole
P_{tube}	pressure measured by sensor-tube
α, β	regression coefficients

References

Irwin HPAH: (1981) "A simple omnidirectional sensor for wind-tunnel studies of pedestrian-level winds", *Journal of Wind Engineering and Industrial Aerodynamics*, **7**, pp219-239.

Kiyota N and Sekine T: (1989) "Experiment study on pressure loss at the opening of wall surface (Part2)", *J. Archt. Plann. Environ. Eng.*, AIJ, 398: pp47-57.

Kurabuchi T, Ohba M, Arashiguchi A and Iwabuchi T: (2000) "Numerical study of airflow structure of a cross-ventilated model building", *The 7th International Conference on Air Distribution in Rooms 'ROOMVENT 2000'*, pp313-318.

Kurabuchi, T. Ohba, M. Endo, T. Akamine, Y. and Nakayama, F: (2004) "Local Dynamic Similarity Model of Cross-Ventilation Part1-Theoretical Framework", *The International Journal of Ventilation*, **2**, (4), pp371-382.

Ohba M, Kurabuchi T, Endo T, Akamine Y, Kamata M and Kurahashi A: (2004) "Local dynamic similarity of cross-ventilation, Part 2 Application of local dynamic similarity model", *The International Journal of Ventilation*, **2**, (4), pp383-393.

Sawachi T, Narita K, Kiyota N, Seto H, Nishizawa S and Ishikawa Y: (2004) "Wind Pressure and Air Flow in a Full-Scale Building Model under Cross Ventilation", *The International Journal of Ventilation*, **2**, (4), pp343-358.

Vickery BJ and Karakatsanis: (1987) "External wind pressure distribution and induced internal ventilation flow in low-rise industrial and domestic structures", *ASHRAE Transactions*, **93**, Part2, pp2198-2213.

Wu H. and Stathopoulos T: (1994) "Further Experiment on Irwin's Surface Wind Sensor", *Journal of Wind Engineering and Industrial Aerodynamics*, **53**, pp441-452.